Coseismic thermal pressurization can notably prolong earthquake recurrence intervals on weak rate and state friction faults: Numerical experiments using different constitutive equations

Yuta Mitsui

Department of Geophysics, Graduate School of Science, Kyoto University, Kyoto, Japan

Kazuro Hirahara

Department of Geophysics, Graduate School of Science, Kyoto University, Kyoto, Japan

Abstract. We add a new perspective to component factors of earthquake cyclicity, namely coseismic thermal pressurization (TP) within fluid-saturated fault zones, which is pore fluid pressurization caused by frictional heating. By using a single degree of freedom system with a rate- and state-dependent friction law, we show that the short-lived TP can prolong earthquake recurrence intervals. This lengthening effect can operate even without any notable shear heating in weak faults. Moreover, if the maximum increase in temperature is above a certain level, the permeability rather than the maximum temperature becomes important for the lengthening effect. Lower permeability causes longer recurrence intervals. By contrast, narrower slip zones (more pronounced heating) do not simply prolong recurrence intervals, although they entail higher dynamic undershoot and energy radiation. These features do not depend on whether the assumed evolution law is the Ruina law or the Dieterich law. However, our results indicate that if the degree of TP changes for each earthquake, the ideal time-predictable model for earthquake cycles can be applicable only in the case of faults obeying the Ruina law. Furthermore, on the basis of the above mentioned dependence of the interval on the permeability, we point out that it is necessary to measure the permeability rather than the slip zone thickness (or the increase in temperature) in order to estimate the TP effect on long-term earthquake cycles. Although it is currently difficult to measure the permeability under ground, measurements should be performed in the light of the importance of permealibility in the prediction of future seismic hazards.

1. Introduction

Although earthquakes are short-lived events, they are preceded by rather long preparation periods. The transition is rapid but seamless.

From this standpoint, *Brace and Byerlee* [1966] proposed that stick-slip behavior is a mechanism for earthquakes. Following this proposition, a number of researchers have conducted numerical calculations for systems with a single degree of freedom or higher space-dimensional elastic systems in order to gain insight into earthquake cyclicity (e.g., *Rice and Tse* [1986], *Gu and Wong* [1991], *Tse and Rice* [1986], *Rice* [1993]). For such studies, it is necessary to use a constitutive law of friction on a fault interface. By way of example, a rate- and state-dependent friction law (*Dieterich* [1979]) has been widely used, because it contains a description of frictional healing during interseismic periods. In recent years, such numerical studies have been developed to model complexities of frictional properties reflecting realistic tectonic settings (e.g., *Kato* [2004], *Liu and Rice* [2007]). These studies are rather important for considering real earthquake cycles, although they lack certain crucial component factors of earthquake cyclicity.

Here, in order to compensate for these shortcomings, we attempt to add a new perspective to the study of earthquake cyclicity, namely the effect of short-term changes in pore fluid pressure due to coseismic thermal pressurization (hereinafter referred to as TP).

TP is a short-lived physical mechanism in which frictional heating at a fluid-saturated fault pressurizes the pore fluid within the fault zone (*Sibson* [1973]). It is considered that this mechanism operates in small-scale volumetric regions of fault systems where a slip is primarily concentrated. In fact, a recent geochemical study on the Chelungpu fault (*Ishikawa et al.* [2008]), which is associated with the 1999 Chi-Chi earthquake, shows that evidence of high-temperature fluid derived from shear heating exists within narrow zones with a thickness of $2 - 15$ cm. Although TP can occur within narrow slip zones, it can greatly affect the constitutive relation of dynamic faults (e.g., *Andrews* [2002], *Suzuki and Yamashita* [2006], *Bizzarri and Cocco* [2006b]) by reducing the normal stress on the friction surface.

In this paper, by using the rate- and state- dependent friction law and a system with a single degree of freedom which is equivalent to a far-field elastic loading system with a spatially uniform fault patch, we show that the short-lived TP is an important mechanism for earthquake cyclicity. Although our analog fault model is simple, it represents the entire earthquake cycle consisting of a long preparation period and a short-lived event with a seamless transition.

Specifically, we investigate the effects of TP under the condition of a weak fault (namely, conditions of low effective normal stress) in the absence of macroscopic rock melting. It can be applicable to realistic fault models. For example, some observational studies have revealed that coseismic heating at the Chelungpu fault is not sufficiently strong for

the rock to melt (*Kano et al.* [2006], *Tanaka et al.* [2006], *Ishikawa et al.* [2008]). Furthermore, certain subduction thrust faults are considered to be weak on grounds of seismic and geodetic data (*Wang* [2000]) or equilibrium of forces (*Seno* [2009]).

In addition, we examine the effects of two different strength evolution laws in the rate and state law in order to avoid discussing the numerical results which are strongly dependent on the evolution laws.

2. Numerical Model

2.1. Constitutive relations

First, we assume a homogeneous fault patch in a uniform infinite elastic body. Spatially uniform relative slip on the fault patch is governed by loading shear stress τ and frictional stress τ_f. The relation between τ, τ_f and the slip velocity v is given by a solution of the equation of motion. In this study, we do not use the ideal equation of motion, which includes an assumption of energy conservation within the system. Rather, we assume quasi-static balance of τ and τ_f accompanying energy lost through elastic wave radiation. Owing to the fundamental approximation of the uniform slip on the fault patch, the amount of stress drop due to elastic wave radiation can be simply represented as $Gv/2c_s$, where c_s is shear wave velocity and G is rigidity. This term, which is the "instantaneous term" (the first term on the right side of equation (8) in *Cochard and Madariaga* [1994]; the sixth term on the right side of equation (3) in *Fukuyama and Madariaga* [1998]), corresponds to the Brune stress drop (*Brune* [1970]) or the radiation damping term in *Rice* [1993]. Therefore the relation is given by:

$$v = (\tau - \tau_f)\frac{2c_s}{G} \tag{1}$$

Next, τ is driven by a far-field steady loading rate v_0 with a corresponding elastic constant k :

$$\tau = k(v_0 t - u) \tag{2}$$

where t is time and u is the amount of total slip.

Subsequently, it is necessary to assume a constitutive law for τ_f, which is generally composed of the frictional coefficient μ and the effective normal stress $\bar{\sigma}$. Regarding the former, we use the laboratory-derived rate- and state-dependent law:

$$\frac{\tau_f}{\bar{\sigma}} = \mu = \left[\mu_0 + b\ln\left(\frac{v_0\theta}{L}\right)\right] + a\ln\left(\frac{v}{v_0}\right) \tag{3}$$

where the term $[\mu_0 + b\ln(v_0\theta/L)]$ represents a dimensionless frictional strength (*Nakatani* [2001]), a is a governing parameter for the direct effect of velocity on friction, and b and L are the governing parameters for the friction evolution. For simplicity, we assume that they are constant through time. There are two major evolution laws for θ. One is the Ruina law (*Ruina* [1983]):

$$\frac{d\theta}{dt} = -\frac{v\theta}{L}\ln\left(\frac{v\theta}{L}\right) \tag{4}$$

The other law is the Dieterich law (*Ruina* [1980]; based on *Dieterich* [1979]) :

$$\frac{d\theta}{dt} = 1 - \frac{v\theta}{L} \tag{5}$$

It is well known that the former provides a more accurate representation of the friction behavior corresponding to velocity changes, while the latter is more suitable for frictional healing (e.g., *Kato and Tullis* [2001]; *Nakatani* [2001]). In this study, we adopt both laws for comparison. In addition, *Linker and Dieterich* [1992] showed on the basis of laboratory experiments that normal stress alteration can affect the evolution of the state θ. We also investigate the effects of the "Linker-Dieterich term" and confirm that it has little influence on the following effects of TP (see Appendix A).

Finally, TP, which is the subject of this study, affects $\bar{\sigma}$. It greatly decreases $\bar{\sigma}$ only during high-speed slip since $\bar{\sigma}$ equals the difference of the normal stress σ and the pore pressure p. When the TP effect is introduced, it is necessary to consider the changes in temperature caused by frictional heating within the slip zone. The degree of frictional heating depends on the thickness of the slip zone. A narrower slip zone entails more concentrated strain and considerable heating, while a wider slip zone entails a more diffuse strain and moderate heating. If the zone is sufficiently narrow, the frictional heating becomes pronounced, and the TP effect can not be ignored. In addition, the degree of TP is also dependent on the diffusivity of the heat and that of the pore fluid.

Under the assumptions of finite and constant thickness of the slip zone, perfect conversion of internal energy into thermal energy (this assumption is supported by a geological study; *Pittarello et al.* [2008]), an isotropic surrounding medium and a constant porosity, the constitutive equations for the temperature and the evolution of the pore pressure at a friction surface (the center of the slip zone) are given by *Bizzarri and Cocco* [2006a]:

$$T(t) = T_0 + \frac{1}{\rho c w}\int_0^t \mathrm{erf}\left(\frac{w}{4\sqrt{\chi(t-t_*)}}\right)\tau_f(t_*)v(t_*)dt_* \tag{6}$$

$$p(t) = p_0 + \frac{\Lambda}{\rho c w}\int_0^t \left[-\frac{\chi}{\varpi-\chi}\mathrm{erf}\left(\frac{w}{4\sqrt{\chi(t-t_*)}}\right) + \frac{\varpi}{\varpi-\chi}\mathrm{erf}\left(\frac{w}{4\sqrt{\varpi(t-t_*)}}\right)\right]\tau_f(t_*)v(t_*)dt_* \tag{7}$$

where $T(t)$ is the temperature at the fault surface at time t, T_0 is a reference value of the temperature at time 0, $p(t)$ is the pore pressure at the fault surface at time t and p_0 is a basic value of the pore pressure at time 0. Note that T_0 is not an important parameter in this study since it is not associated with the other parameters in our calculations. Also, ρ and c represent the density and the specific heat of the bulk composite, respectively, w is the thickness of the slip zone, χ is the temperature diffusivity, which is equivalent to $\lambda/[\rho c]$, where λ is the bulk thermal conductivity, Λ is an expansion ratio defined as $[\alpha_f - \alpha]/[\beta_f + \beta]$, where α_f is the thermal expansivity of the pore fluid and α is that of the solid, while β_f is the compressibility of the pore fluid and β is that of the solid. Finally, ϖ is the pressure diffusivity, which is equal to $\kappa/[(\beta_f + \beta)\phi\nu_f]$, where κ is the permeability, ϕ is the porosity, ν_f is the viscosity of the pore fluid, and erf() is the error function.

In addition, if the thickness of the slip zone is sufficiently small to be regarded as zero, the equations (6) and (7) can be simplified (*Rice* [2006], *Bizzarri and Cocco* [2006a]) as follows:

$$T(t) = T_0 + \left(1 + \sqrt{\frac{\varpi}{\chi}}\right)\frac{p(t) - p_0}{\Lambda} \tag{8}$$

Table 1. Common parameters in this study.

Property	Symbol	Value	Units
Shear wave velocity	c_s	3500	m/s
Rigidity	G	34.3	GPa
Loading rate	v_0	0.03	m/year
Normal stress	σ	0.15	GPa
Reference pore pressure	p_0	0.14	GPa
Frictional coefficient	μ_0	0.6	
Friction parameter	a	0.01	
Friction parameter	b	0.015	
Friction parameter	L	0.02*	m
Background temperature	T_0	473	K
Bulk density	ρ	2800	kg/m^3
Bulk specific heat	c	1.0×10^3	J/(kg·K)
Bulk thermal conductivity	λ	2.0	W/(m·K)
Solid thermal expansivity	α	-1.0×10^{-4}	/K
Fluid thermal expansivity	α_f	5.0×10^{-4}	/K
Solid compressibility	β	1.0×10^{-9}	/Pa
Fluid compressibility	β_f	1.0×10^{-10}	/Pa
Porosity	ϕ	0.01	
Fluid viscosity	ν_f	1.0×10^{-4}	Pa·s

* This value is not derived from a laboratory experiment but from a seismic inversion (*Guatteri et al.* [2001]).

$$p(t) = p_0 + \frac{\Lambda}{2\sqrt{\pi}\rho c(\sqrt{\chi}+\sqrt{\varpi})}\int_0^t \frac{\tau_f(t_*)v(t_*)dt_*}{\sqrt{t-t_*}} \quad (9)$$

In the numerical calculations, as initial values, we set a steady state condition as $v = 0.1v_0$, $\theta = L/[0.1v_0]$, $p = p_0$ and $T = T_0$. To solve the above constitutive relations, first we integrate the coupled equations (1)-(4) by using RK45, which is a Runge-Kutta method with adaptive step-size control (*Press et al.* [1992]). Then, we calculate the pore pressure value from equation (7) or (9), and, at the next time step, we solve the coupled equations (1)-(4) by using the calculated pore pressure. All memories of the temperature and the pore pressure during a single high-speed event for calculating (1)-(4) are preserved for the next event. However, when the slip velocity does not exceed the loading rate v_0, we ignore the shear heating. This is not an artificial assumption since p_0 and T_0 reflect the pore pressure and the temperature in the steady condition, respectively, although there remains the slight problem that p_0 and T_0 are initial parameters with $v = 0.1v_0$. In fact, this problem is not important in this study because the degree of TP can be ignored during interseismic periods with such the low slip velocity. We describe it in Appendix B.

2.2. Model parameters

First, we assume realistic model parameters by referring to previous studies. The common parameters used in all experiments are provided in Table 1. In particular, the weakness of the model fault is important. A stronger fault leads to more intense shear heating, while a weaker fault leads to moderate heating. In this paper, we assume a weak fault with low effective normal stress, as mentioned in Section 1. The value of $\sigma - p_0$ is set to 10 MPa.

Regarding the elastic stiffness k, in order to produce stick-slip behavior, we also set a constant value k_1:

$$k_1 = 0.5\frac{(\sigma - p_0)(b-a)}{L} \quad (10)$$

On the other hand, we can interpret k in terms of the shear crack theory in an infinite elastic medium. Under the simple assumption that the Poisson ratio is 0.25 and the homogeneous fault patch is circular, the effective elastic stiffness k is generally written as $[7\pi/24][G/r]$ (*Eshelby* [1957]), where r is the radius of the circular patch. If we assign k_1 to this relation, we obtain

$$r_1 = \frac{7\pi}{12(\sigma - p_0)}\frac{GL}{(b-a)} \quad (11)$$

This equation (11) implies that our model corresponds to a model of a homogeneous circular crack with a radius r_1. The value of r_1 is approximately 25 km.

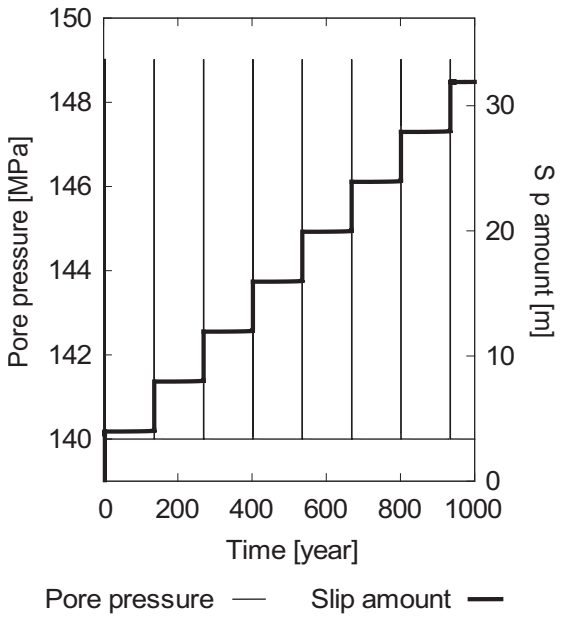

Figure 1. An example of the entire calculated earthquake cycle for the case where we set $w = 4$ cm and $\kappa = 10^{-19}$ m^2 and we use the Ruina evolution law. Theere is a repeated and rapid increase and decrease in pore pressure (thin line) as the slip amount (thick line) suddenly increases. The recurrence interval is 133.0 years.

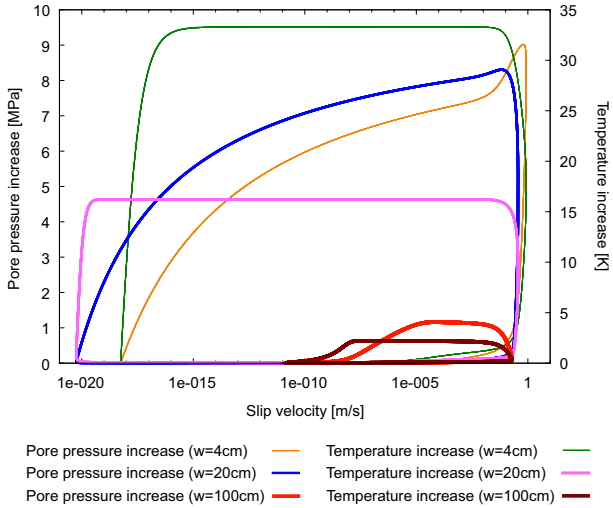

Figure 2. Evolutions of the pore pressure and the temperature of multiple earthquake cycles in the case where we assume $\kappa = 10^{-19}$ m^2 and the Ruina evolution law, with $w = 4$ cm (the same as for Figure 1), $w = 20$ cm and $w = 100$ cm. All of the traces rotate counter-clockwise.

The rest of the parameters are the slip zone thickness w and the permeability κ. A number of previous studies (e.g., *Lachenbruch* [1980], *Mase and Smith* [1987]) have revealed that these parameters exert considerable influence on TP. Moreover, it is difficult to determine these values unambiguously, since the former can not be observed directly at any fault and the latter fluctuates widely even within a same fault belt (e.g., *Wibberley and Shimamoto* [2003], *Tsutsumi et al.* [2004]). Therefore, we change both values and investigate their effects.

Table 2. Model parameters and numerical results in the case of the ill-drained condition $\kappa = 10^{-19}$ m^2 with the Ruina evolution law: Recurrence interval R_i, dynamic stress drop $S_d^\dagger$, static stress drop $S_s^\dagger$, maximum increase in temperature ΔT, amount of coseismic slip u_{cos}, apparent stress $\sigma_a^\ddagger$ and effective moment magnitude $M^\ddagger$.

w [m]	R_i [year]	S_d [MPa]	S_s [MPa]	ΔT [K]	u_{cos} [m]	σ_a [MPa]	M
ϵ^*	126.1	5.6	4.6	200	3.7	3.0	7.5
0.01	127.8	5.6	4.7	95	3.7	2.9	7.5
0.02	129.9	5.6	4.7	57	3.8	2.8	7.5
0.04	133.0	5.7	4.9	33	3.9	2.7	7.5
0.1	141.8	5.7	5.2	20	4.2	2.1	7.6
0.2	141.1	5.3	5.2	16	4.1	1.3	7.6
0.4	97.3	3.5	3.5	9.2	2.8	0.7	7.5
1.0	46.5	1.6	1.6	2.2	1.3	0.5	7.2
2.0	37.9	1.3	1.3	0.9	1.0	0.4	7.2
∞^{**}	32.0	1.1	1.1	0.0	0.9	0.4	7.1

† See subsection 3.1.2.
‡ See subsection 4.3.
* Limit of zero thickness slip zone.
** No TP effect (no shear heating).

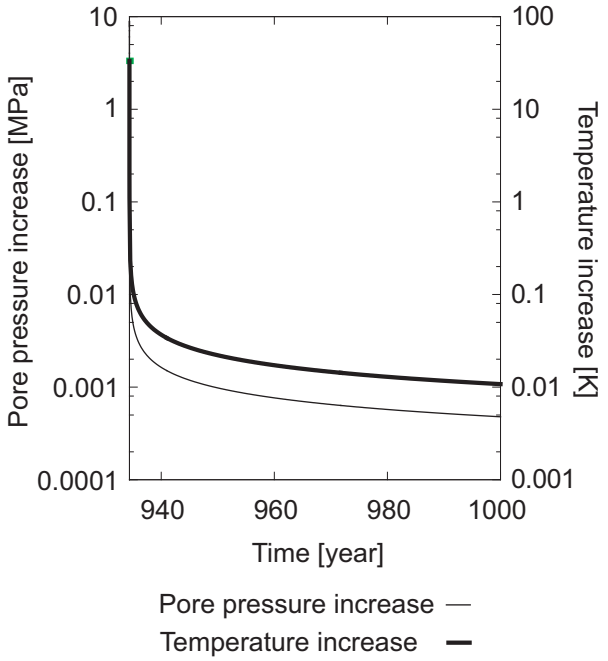

Figure 3. Evolutions of the increase in pore pressure $p - p_0$ and the increase in temperature $T - T_0$ during one co- and post-seismic period, under the same setting as that for Figure 1. Both evolutions are plotted immediately after the slip velocity reaches its maximum value. The maximum increase in pore pressure is 9.0 MPa and the increase in temperature is 33 K.

3. Results

Our numerical experiments exhibit a stick-slip behavior, which can be interpreted as the entire earthquake cycle. One example is shown in Figure 1. Regular slip events occur at a recurrence interval together with the instant increase in the pore pressure. Moreover, Figure 2 illustrates the increase in pore pressure and the increase in temperature during multiple earthquake cycles. The evolutions trace stable cycles, which indicates that we have succeeded in modeling cyclic earthquakes including the TP effect.

3.1. Ill-drained condition with the Ruina law

Initially, as a reference, we present the results for the case of an ill-drained condition $\kappa = 10^{-19}$ m^2 and the Ruina evolution law. For instance, apart from the above-mentioned examples under this assumption (Figures 1-2), the evolution $\Delta p = p - p_0$ of the increase in pore pressure, and that for the increase in temperature $\Delta T = T - T_0$ during a single co- and post-seismic period are presented in Figures 3-4, and additionally the slip velocity evolutions are presented in Figure 5. Figures 2-5 reveal the qualitative nature of our results. The increase in pore pressure and the increase in temperature become more pronounced as the slip velocity approaches its maximum, after which they decrease more gradually than the slip velocity. The residual increase in pore pressure greatly affects the evolution of the slip velocity during the early post-seismic period. This implies that geodetically observed post-seismic slip phenomena (e.g., *Miyazaki et al.* [2004]) might be significantly affected by TP. This intriguing problem will be the focus of our future work.

The compiled results of our numerical experiments are listed in Table 2. It is clear from the table that the TP effect greatly prolongs the recurrence interval. The increase in temperature ΔT becomes more pronounced as w becomes smaller, as revealed by previous studies, although the recurrence interval R_i is not simply prolonged as w becomes smaller. These characteristics are presented in Figure 6.

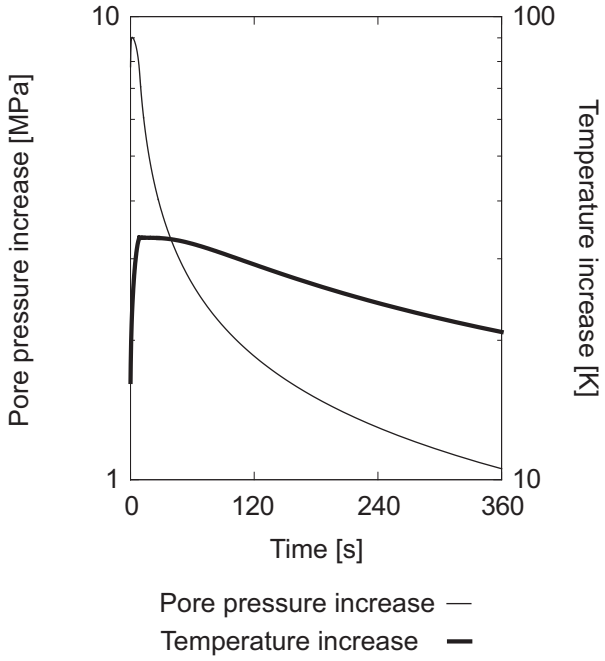

Figure 4. The same as Figure 3 with the exception that the time range is limited to only six minutes. The horizontal axis represents the relative time from the moment when the slip velocity reaches its maximum value.

3.1.1. Increase in temperature and recurrence interval

Note in passing that the recurrence interval becomes rather prolonged as the temperature increases slightly, when the slip zone is not exceedingly narrow. For example, in the case of $w = 0.4$ m, although the increase in temperature is only less than 10 K, the recurrence interval is approximately three times as long as that in the case of $w = \infty$ (no shear heating and no TP effect). By contrast, when the slip zone is sufficiently narrow, the increase in temperature becomes much more pronounced as w becomes smaller, while the recurrence interval peaks out and decreases slightly. This peculiar decrease is due to the characteristics of the friction evolutions, as shown in the following section 3.1.2.

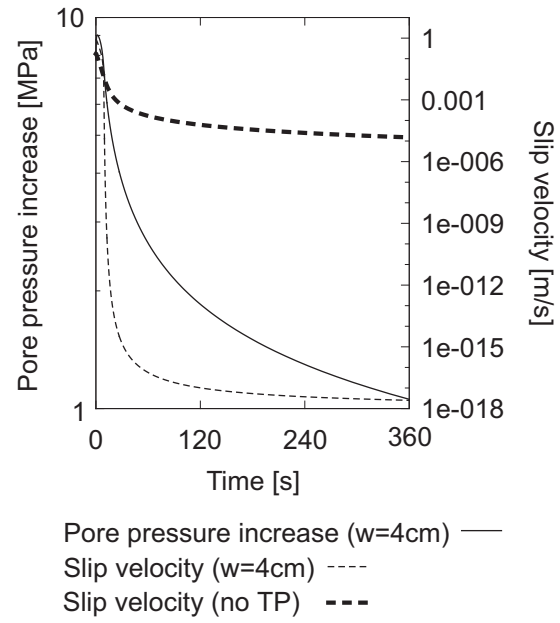

Figure 5. Evolutions of the increase in pore pressure $p - p_0$ and the slip velocity v during co- and post-seismic periods when we assume $\kappa = 10^{-19}$ m^2 and the Ruina evolution law, with $w = 4$ cm (the same as for Figures 1, 3, 4) and without TP. The horizontal axis represents the relative time from the moment when the slip velocity reaches its maximum value in each setting.

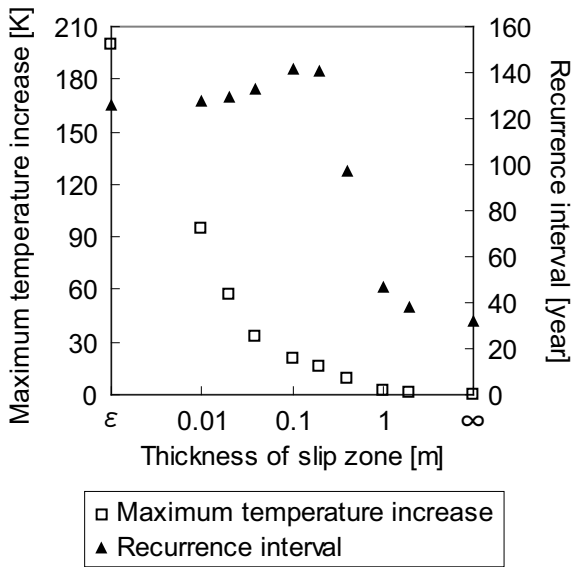

Figure 6. Relations between the slip zone thickness w, the maximum increase in temperature and the recurrence interval in case of the ill-drained condition $\kappa = 10^{-19}$ m^2 with the Ruina evolution law.

3.1.2. Stress drop and recurrence interval

The static stress drop S_s in Table 2 is defined as the difference between the maximum frictional stress immediately before the earthquake with a certain accelerated velocity and the dropped frictional stress with a certain decelerated velocity. In this study, the threshold values of both the slip velocities for defining S_s are the same: the loading rate v_0. Furthermore, we define the dynamic stress drop S_d as the difference between the maximum frictional stress immediately before the earthquake and the minimum stress during the earthquake, with the slip velocity exceeding the loading rate v_0. These results are illustrated in Figure 7.

From Table 2, it is clear that the recurrence interval R_i is roughly proportional to the static stress drop S_s. Figure 8 represents this result.

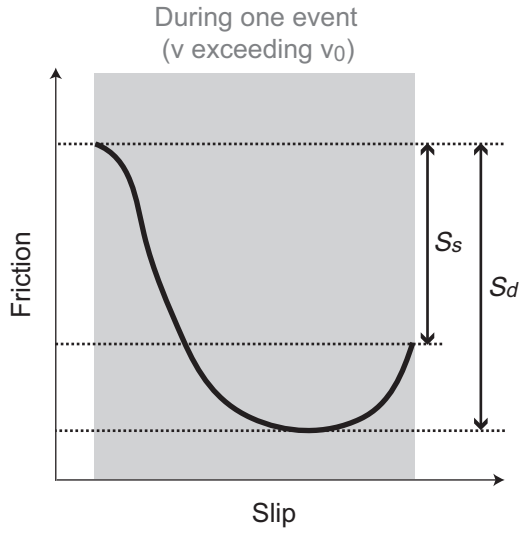

Figure 7. Static stress drop S_s and dynamic stress drop S_d in this study.

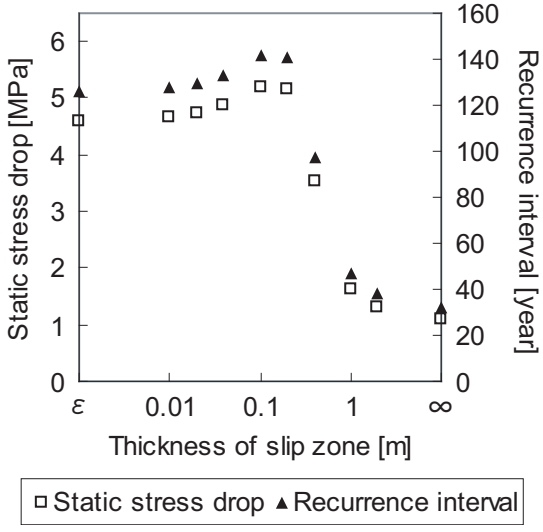

Figure 8. The same as Figure 6 with the exception of the static stress drop instead of the maximum increase in temperature.

The next question is why the recurrence interval or the static stress drop is shorter or smaller when w is sufficiently small. Before considering this issue, it should be mentioned that the dynamic stress drop S_d would also peak when w is sufficiently small, although in fact it does not decrease in the same way as the static stress drop S_s. Figure 9 illustrates this fact. It indicates that dynamic undershoot, where the dynamic stress drop becomes larger than the static drop, occurs in the case when w is sufficiently small.

Thus, we focus on the evolution of the frictional stress τ_f as well as on the evolution of the loading stress τ, since the slip velocity reflects the difference between these parameters in our system (see equation (1)).

As an example, Figure 10 illustrates the case without TP and the case with TP (w = 2 cm). It shows how the static stress drop is increased by TP. Once the earthquake occurs, that is, when the friction τ_f begins to drop obeying the rate and state friction law, TP drastically reduces the friction $\tau_f = \mu(\sigma - p)$ by increasing p, as already shown in a three-dimensional dynamic rupture simulation (*Bizzarri and Cocco* [2006b]), and the loading stress τ drops following τ_f. Then, the friction begins to recover due to the diffusion of the heat and the pore pressure. This process of friction recovery causes a dynamic undershoot. When the loading

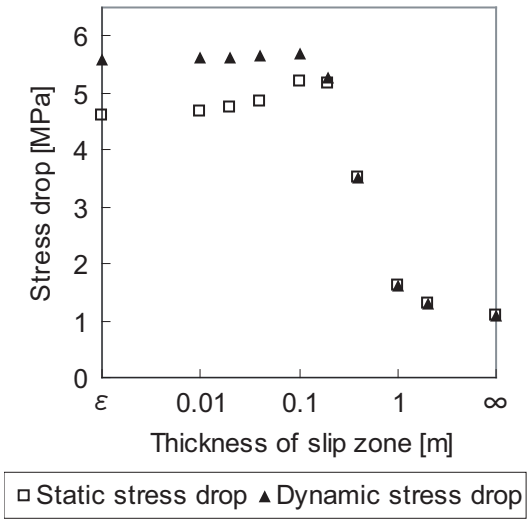

Figure 9. Relations between the thickness w of the slip zone, the static stress drop and the dynamic stress drop in the case of the ill-drained condition $\kappa = 10^{-19}$ m^2 with the Ruina evolution law.

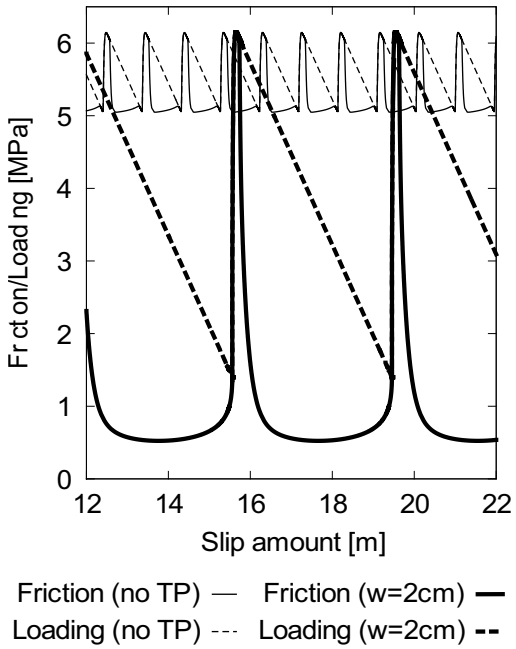

Figure 10. Evolutions of the frictional stress and the loading stress when we set $\kappa = 10^{-19}$ m^2, and we use the Ruina evolution law without TP ($w = \infty$) and with TP ($w = 2$ cm). The horizontal axis represents the total amount of slip from the initial state.

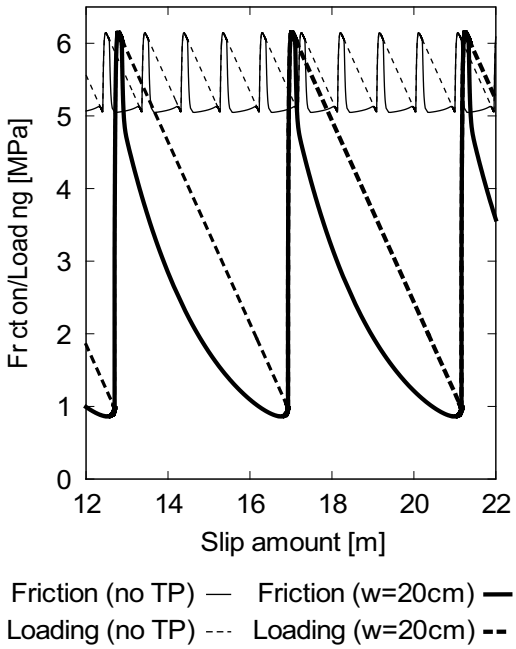

Figure 11. The same as Figure 10 with the exception of the thickness of the slip zone $w = 20$ cm.

Table 3. Model parameters and numerical results in the cases of the better-drained condition $\kappa = 10^{-18}$ m^2 and $\kappa = 10^{-17}$ m^2.

$\kappa = 10^{-18}$ m^2							
w [m]	R_i [year]	S_d [MPa]	S_s [MPa]	ΔT [K]	u_{cos} [m]	σ_a [MPa]	M
ϵ	97.0	4.4	3.5	443	2.8	2.2	7.5
0.01	97.6	4.5	3.5	194	2.8	2.2	7.5
0.02	98.5	4.4	3.6	108	2.9	2.1	7.5
0.04	99.5	4.4	3.6	57	2.9	2.0	7.5
0.1	100.5	4.2	3.6	27	2.9	1.7	7.5
0.2	96.2	3.8	3.5	15	2.8	1.2	7.5
0.4	76.3	2.8	2.7	7.8	2.2	0.7	7.4
1.0	45.8	1.6	1.6	2.2	1.3	0.5	7.2
2.0	37.6	1.3	1.3	0.9	1.0	0.4	7.2
∞	32.0	1.1	1.1	0.0	0.9	0.4	7.1
$\kappa = 10^{-17}$ m^2							
ϵ	50.7	2.1	1.8	420	1.5	0.9	7.3
0.01	50.8	2.1	1.8	187	1.5	0.9	7.3
0.02	50.9	2.1	1.8	103	1.5	0.9	7.3
0.04	50.8	2.1	1.8	52	1.5	0.9	7.3
0.1	50.3	2.0	1.8	21	1.4	0.8	7.3
0.2	49.1	1.9	1.7	11	1.4	0.8	7.2
0.4	46.7	1.8	1.6	5.3	1.3	0.6	7.2
1.0	41.3	1.4	1.4	2.0	1.2	0.5	7.2
2.0	37.1	1.3	1.3	0.9	1.0	0.4	7.2
∞	32.0	1.1	1.1	0.0	0.9	0.4	7.1

stress becomes equal to the frictional stress, the earthquake finishes and the accumulation of quasi-static stress is resumed.

Here, we can discuss why the recurrence interval or the static stress drop becomes shorter or smaller when w is sufficiently small. The most probable reason is that when w is sufficiently small, it leads to the faster decrease of the friction and the its earlier "plateau" (limit by the absolute level of initial friction) as well as the later process of catching up with the loading stress of the friction recovery. In fact, as shown in Figure 11, when w is moderately small ($w = 20$ cm in this case), the friction decrease is relatively gentle and dynamic undershoot almost does not arise.

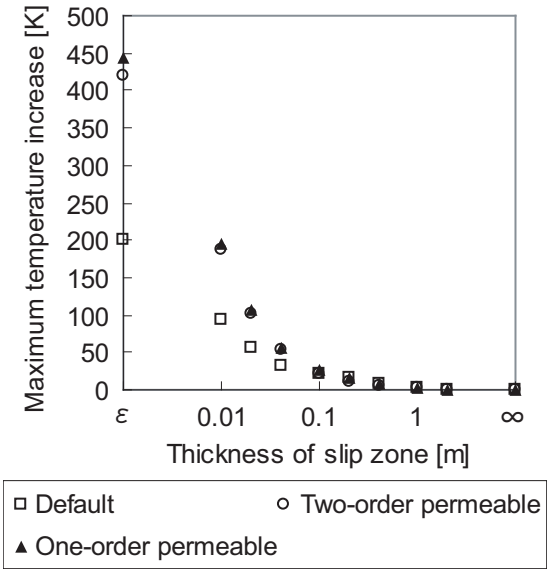

Figure 12. Relations between the thickness w of the slip zone and the maximum increase in temperature for the cases of the default (ill-drained) condition $\kappa = 10^{-19}$ m^2, the one-order permeable condition $\kappa = 10^{-18}$ m^2 and the two-order permeable condition $\kappa = 10^{-17}$ m^2, with the Ruina evolution law in each case.

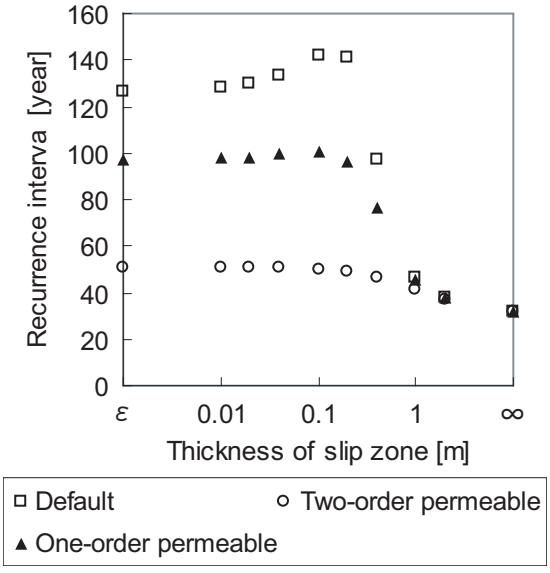

Figure 13. The same as Figure 12 with the exception of the recurrence interval instead of the maximum increase in temperature.

3.2. Better-drained condition with the Ruina law

Next, we address the results with the better-drained conditions, $\kappa = 10^{-18}$ m^2 and $\kappa = 10^{-17}$ m^2, together with the Ruina evolution law.

The results of our numerical experiments are listed in Table 3. It is clear that the reccurrence intervals are not

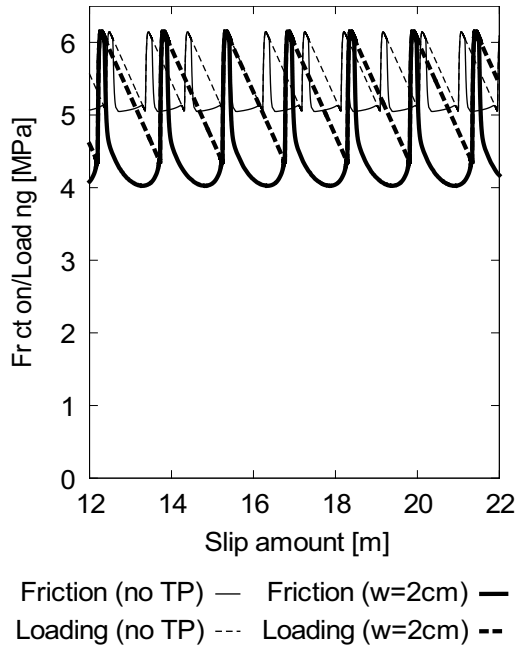

Figure 14. Evolutions of the frictional stress and the loading stress when we set $\kappa = 10^{-17}$ m^2 and use the Ruina evolution law without TP ($w = \infty$) and with TP ($w = 2$ cm). The horizontal axis represents the total amount of slip from the initial state.

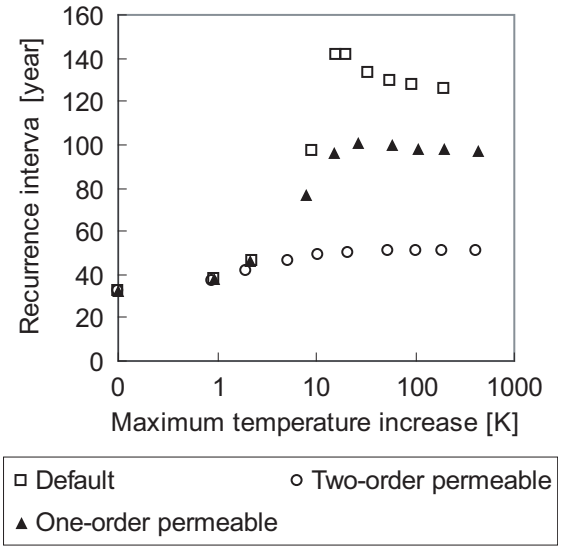

Figure 15. Relations between the maximum increase in temperature and the recurrence interval for comparison between the cases of the default (ill-drained) condition $\kappa = 10^{-19}$ m^2, the one-order permeable condition $\kappa = 10^{-18}$ m^2 and the two-order permeable condition $\kappa = 10^{-17}$ m^2, with the Ruina evolution law in each case.

prolonged as much by TP as in the case with the ill-drained condition, $\kappa = 10^{-19}$ m^2.

In order to perform a comparison with the ill-drained condition, the characteristics of the temperature increase, and the recurrence intervals are illustrated in Figures 12 and 13, respectively. It is noteworthy that the sufficiently high permeability restrains the effects of TP on the recurrence interval. This restraining is naturally due to the higher speed of the pressure diffusion. In fact, Figure 14 shows that even with a sufficiently small w, $w = 2$ cm, the friction weakening due to TP can not be as pronounced as that in the case with the ill-drained condition (Figure 10).

Furthermore, we rewrite the above results as a relationship between the increase in temperature ΔT and the recurrence interval R_i, and show the results in Figure 15. Here, we see that there might be a boundary at $\Delta T \sim$ a few degrees below 10 K. If ΔT exceeds it, R_i can be significantly prolonged by TP depending on the permeability. In contrast, if ΔT falls much below it, R_i is not notably prolonged for any permeability in the examined range.

3.3. Difference between cases with the Ruina law and cases with the Dieterich law

Finally, we consider the cases with the Dieterich evolution law. The results are listed in Table 4.

It is clear that the characteristics of the results are very similar to those with the Ruina law, although the values of the maximum increase in temperature and the stress drop are slightly larger. With either law, the recurrence interval is almost linearly proportional to the static stress drop (Figure 16). TP, independently of the state evolution laws, determines the simple relation between them. It is far from a scaling of the stress drop with the logarithm of the recurrence interval as reported in a previous numerical study (*He et al.* [2003]). Since their model and ours are slightly different in terms of the definition of stress drop and the treatment of dynamic effects, we would further investigate this point in future studies.

The only difference which we find is whether TP affects the maximum friction immediately before the earthquake.

Table 4. Model parameters and numerical results in the case of the Dieterich evolution law.

w [m]	R_i [year]	S_d [MPa]	S_s [MPa]	ΔT [K]	u_{cos} [m]	σ_a [MPa]	M
			$\kappa = 10^{-19}$ m^2				
ϵ	136.8	6.1	5.1	202	4.1	3.1	7.6
0.01	138.5	6.1	5.1	98	4.2	3.0	7.6
0.02	140.6	6.1	5.2	60	4.2	2.9	7.6
0.04	143.8	6.1	5.3	35	4.3	2.8	7.6
0.1	152.8	6.2	5.7	21	4.6	2.3	7.6
0.2	154.7	5.9	5.7	17	4.6	1.5	7.6
0.4	114.9	4.3	4.3	11	3.4	0.8	7.5
1.0	55.7	2.0	2.0	2.8	1.6	0.5	7.3
2.0	43.4	1.6	1.6	1.2	1.3	0.4	7.2
∞	34.8	1.3	1.2	0.0	1.0	0.3	7.2
			$\kappa = 10^{-18}$ m^2				
ϵ	107.9	5.0	4.0	459	3.2	2.2	7.5
0.01	108.6	5.0	4.0	205	3.3	2.2	7.5
0.02	109.5	5.0	4.1	116	3.3	2.2	7.5
0.04	110.7	4.9	4.1	62	3.3	2.1	7.5
0.1	112.3	4.8	4.2	29	3.3	1.8	7.5
0.2	109.7	4.4	4.1	17	3.2	1.3	7.5
0.4	91.0	3.5	3.4	9.3	2.7	0.8	7.4
1.0	54.3	2.0	2.0	2.7	1.6	0.4	7.3
2.0	42.9	1.6	1.6	1.1	1.3	0.4	7.2
∞	34.8	1.3	1.2	0.0	1.0	0.3	7.2
			$\kappa = 10^{-17}$ m^2				
ϵ	59.0	2.6	2.2	471	1.8	0.9	7.3
0.01	59.2	2.6	2.2	214	1.8	0.9	7.3
0.02	59.2	2.6	2.2	120	1.8	0.9	7.3
0.04	59.2	2.5	2.2	61	1.8	0.8	7.3
0.1	58.6	2.5	2.1	25	1.8	0.8	7.3
0.2	57.2	2.4	2.1	13	1.7	0.6	7.3
0.4	54.3	2.1	2.0	6.5	1.6	0.6	7.3
1.0	47.5	1.8	1.7	2.4	1.4	0.4	7.3
2.0	42.0	1.5	1.5	1.1	1.2	0.4	7.2
∞	34.8	1.3	1.2	0.0	1.0	0.3	7.2

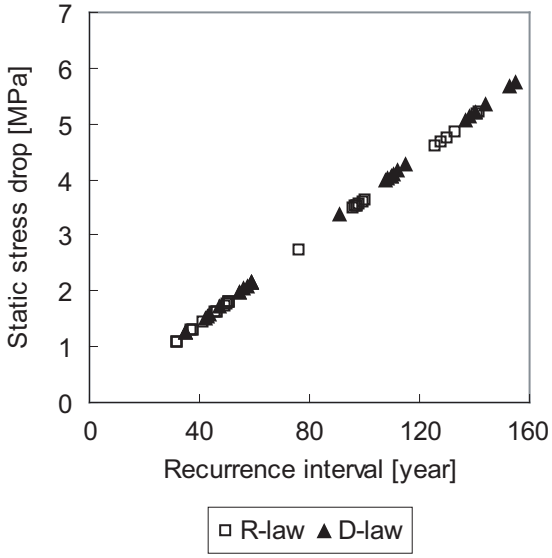

Figure 16. Relations between the recurrence interval and the static stress drop for all cases in Tables 2-4. Open rectangles (R-law) represent the cases with the Ruina evolution law and solid triangles (D-law) represent the cases with the Dieterich evolution law.

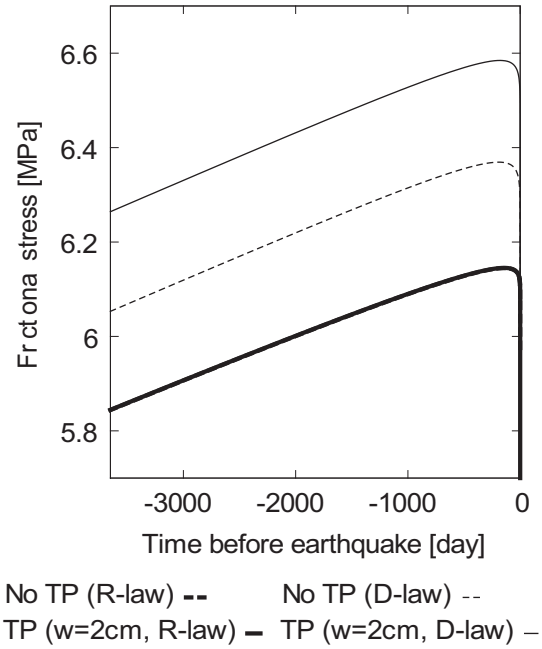

Figure 17. Temporal evolutions of the frictional stress when we use the Ruina evolution law (R-law) and the Dieterich evolution law (D-law) without TP ($w = \infty$) and with TP ($w = 2$ cm and $\kappa = 10^{-19}$ m^2). Horizontal axis represents the time before each earthquake. Note that the thick dashed line is fully hidden underneath the thick solid line.

We focus on the behavior of the friction during the ten years preceding the seismic period and present the results in Figure 17. In the cases with the Ruina law, the friction evolutions are almost the same regardless of TP. By contrast, in the cases with the Dieterich law, the friction evolutions are changed by TP. Namely, TP can increase the maximum friction only in the case with the Dieterich law.

This difference is due to the difference of the evolution law of the dimensionless frictional strength, $\Theta = [\mu_0 + b\ln(v_0\theta/L)]$. The magnitude relation between Θ and the frictional coefficient μ controls the slip velocity (*Nakatani* [2001]):

$$v = v_0 \exp\left(\frac{\mu - \Theta}{a}\right) \tag{12}$$

where equation (12) is an expression for equation (3). The frictional coefficient μ must exceed the dimensionless frictional strength Θ for the earthquake to begin. Figure 18 shows the evolutions of the dimensionless frictional strength throughout the earthquake cycles. The red and black lines in Figure 18 reveal why the maximum friction during the earthquake cycle is increased by TP in the case with the Dieterich law. It is rather straightforward that the dimensionless frictional strength Θ increases almost logarithmically with time t during the interseismic period (the period with extremely low v) by following the relation $\theta \sim t$ (see equation (5)). Thus, in the case of the Dieterich law, the longer recurrence interval simply increases the maximum dimensionless frictional strength and the coefficient immediately before the earthquake. By contrast, in the case of the Ruina law, the dimensionless frictional strength immediately before the earthquake is scarcely affected by TP, as represented by the thick lines in Figure 18. This result is somewhat surprising. Incidentally, in the case of TP (thick-solid red line), strength healing hardly occurs during the early interseismic period. This might be due to the extremely low slip velocity during that period (Figure 19), since the strength evolution of the Ruina law, equation (4), does not present its healing as in the case of the Dieterich law but instead remains in the range of extremely low values of v.

Thus, we discovered an interesting phenomenon where TP increases the maximum friction on faults obeying the Dieterich law (Dieterich faults), while this phenomenon does not take place in faults obeying the Ruina law (Ruina faults), as shown in Figure 18. The ideal time-predictable model for earthquake cycles as proposed by *Shimazaki and Nakata* [1980] has a certain fixed value of the frictional strength throughout earthquake cycles. Interestingly, it appears that the Ruina fault has a fixed value of the dimensionless frictional strength regardless of the presence of TP. However, in Dieterich faults, the dimensionless frictional strength is different in each earthquake cycle if the degree of TP for each earthquake event changes.

Although the question whether such fluctuations of TP can occur has not yet been answered, it is impossible to determine whether the degree of TP is almost constant across multiple earthquake cycles. Furthermore, it is likely that the degree of TP tends to be small as the earthquake events occur repeatedly, since the thicknesses of fault zone components are considered to have a positive trend for total fault displacement (e.g., *Shiption et al.* [2006]).

Indeed, the difference in maximum strength is not as large as seen in our simulation. However, strictly speaking, the time-predictable model is applicable only to Ruina faults, and not to Dieterich faults, if each earthquake event is affected by TP to a different extent.

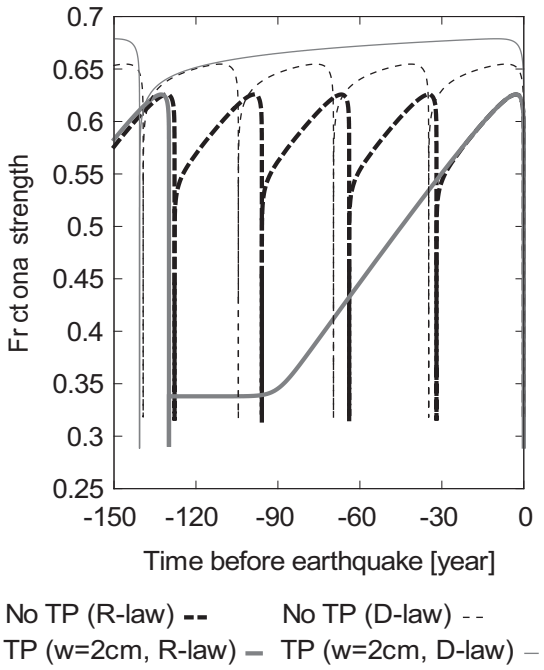

Figure 18. Temporal evolutions of the dimensionless frictional strength when we use the Ruina evolution law (R-law) and the Dieterich evolution law (D-law) without TP ($w = \infty$) and with TP (w = 2 cm and $\kappa = 10^{-19}$ m^2). Horizontal axis represents the time in years before each earthquake.

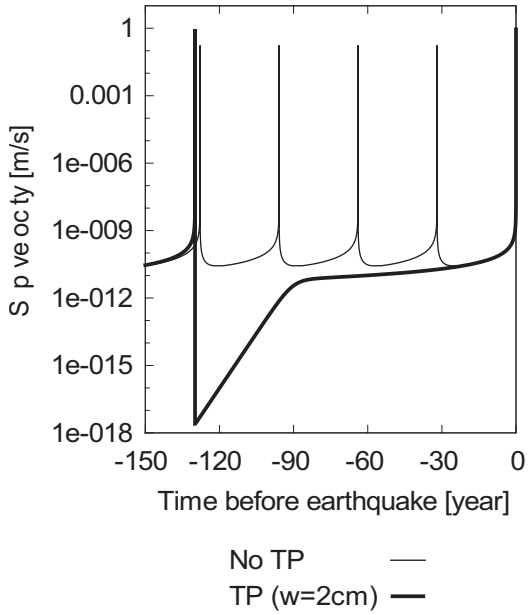

Figure 19. Temporal evolutions of the slip velocity when we use the Ruina evolution law without TP ($w = \infty$) and with TP (w = 2 cm and $\kappa = 10^{-19}$ m^2). Horizontal axis represents the time in years before each earthquake.

4. Discussion

Care should be taken as to how our numerical model calculations based on the simple model under several assumptions are applicable to real earthquakes.

4.1. Dimensionality problem

One important point is that our simple model assumes a homogeneous slip on the fault patch. Due to this assumption, our system with a single degree of freedom can not represent local stress concentration at rupture fronts, which is different from cases for higher space-dimensional elastic systems. The non-stress concentration leads to underestimation of the degree of increase in temperature due to lower slip velocity. Therefore, it should be noted that our model would completely underestimate the degree of TP.

4.2. Comparison with geologic observations

Recently, geochemical studies on the Chelungpu fault (*Ishikawa et al.* [2008]) have revealed that thermal pressurized fluids might exist in the intensely sheared bands with thickness of $0.02 - 0.15$ m.

In addition, a review of geological observations (*Sibson* [2003]) reports that coseismic shearing is localized in a region of less than 0.1 m in planar faults throughout the crustal seismogenic zone. Following these observations, the thickness w of the slip zone would be hardly more than 0.15 m.

Hence, it is likely that our results with $w > 0.15$ m can be safely ignored since it appears that such wide slip zones are unrealistic. Figure 13 shows that under realistic conditions with $w < 0.15$ m, the recurrence intervals depend on the permeability κ rather than on the thickness w of the slip zone. This implies that the permeability rather than the thickness of the slip zone (or the increase in temperature) should be measured in order to estimate the effects of TP on the long-term earthquake cycle.

Naturally, the above inference relies on the assumption of a weak fault, since fundamental weakness of the fault causes the "plateau" of the stress drop and the recurrence interval. Originally, we assume the weak fault model as the model on which shear heating is not sufficient for macroscopic rock melting to occur. This assumption is appropriate for considering faults in which there is almost no evidence of melting such as the Chelungpu fault (*Tanaka et al.* [2006]). However, there most certainly exist faults with clear evidence of melting or fluidization of gouges such as the Nojima fault, which is associated with the 1995 Hyogoken-nambu earthquake (*Otsuki et al.* [2003]). Since the melting or the fluidization can drastically alter the fault constitutive relation of the fault (*Hirose and Shimamoto* [2005], *Brodsky and Kanamori* [2001]), we should regard such faults with considerable heating as distinct entities.

4.3. Comparison with seismic observations

To a limited extent, we can estimate the effects of TP on seismically observable parameters. For example, we can derive the effective moment magnitude M from the amount of coseismic slip amount and the concept of the effective crack radius r_1 (cf. equation (11)). Naturally, it is only controlled by the static stress drop in our 1D model. We calculate it by using $M = (\ln M_o - 9.1)/1.5$, where the effective seismic moment M_o is given by $Gu_{cos}\pi r_1^2$. Our results in Tables 2-5 show that M ranges between 7.1 and 7.6 and increases up to by 0.5 due to TP. It would be a rough estimate for the degree of TP on the moment magnitude around 7.

Furthermore, we calculate the apparent stress σ_a, which is equivalent to the radiated energy per unit area divided by the amount of coseismic slip (e.g., *Kanamori and Rivera* [2006]). Since the radiated energy per unit area during the coseismic slip can be derived in this one-dimensional setting, σ_a can be estimated. Here, we approximate the radiated energy per unit area as $\int[\tau(t) - \tau_f(t)]v(t)dt$. This approximation is acceptable in our simple model since τ decreases almost linearly during the coseismic slip via the constant stiffness k (see Figures 10, 11 and 14). Again, the threshold velocity of the coseismic slip is the loading rate v_0. From our results in Tables 2-5, σ_a increases by a factor of up to 10 due to TP, which provides a rough estimate for the degree of the effect of TP on the apparent stress.

Figure 20 illustrates an example of the relation among the slip zone thickness w, the effective moment magnitude M and the apparent stress σ_a in the case of the ill-drained condition. Smaller w leads to larger apparent stress, unlike the static stress drop (and the moment).

The above estimations for the effective moment magnitude and the apparent stress allow us to compare our results with results from seismic observations. As a reference, based on a number of analyses of actual earthquakes, several studies (e.g., *Brodsky and Kanamori* [2001], *Mayeda et al.* [2005]) have suggested that scaled energy, equivalent to σ_a/G, in large earthquakes are greater than those in small earthquakes. This implied non-self-similarity of earthquakes might correspond to velocity-dependent weakening mechanisms such as TP.

However, it should be noted that the apparent stress σ_a is inversely correlated with the effective moment magnitude M_o (or the static stress drop) when we ignore the results with $w > 0.15$ m in Figure 20 from the geological constraints, as noted in section 4.2. Due to the plateauing of the static stress drop, the effect of TP on the energy-moment relation is not as simple as to cause a positive correlation between them.

5. Conclusion

To our knowledge, the present study provides the first statement that, under several assumptions, TP can prolong the earthquake recurrence interval. We also confirm that TP alters the friction evolution at fluid-saturated faults, accelerates the fault slip and increases the stress drop, as already demonstrated in earlier studies using different fault models

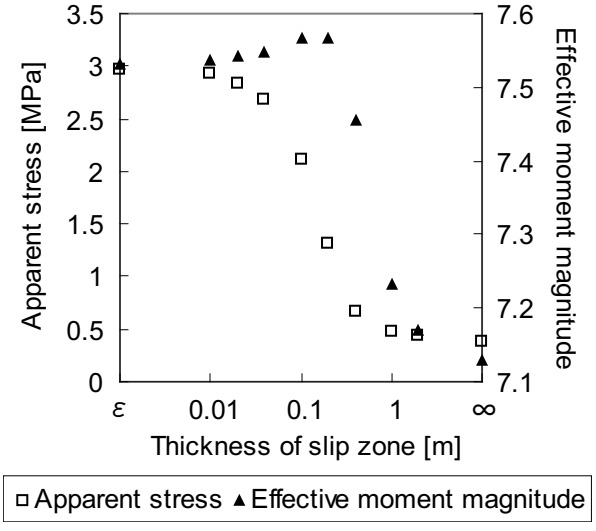

Figure 20. Relations between the thickness w of the slip zone, the apparent stress σ_a and the effective moment magnitude M in the case of the ill-drained condition $\kappa = 10^{-19}$ m^2 with the Ruina evolution law.

(e.g., *Andrews* [2002], *Suzuki and Yamashita* [2006], *Bizzarri and Cocco* [2006b]).

This lengthening effect can certainly operate even without notable shear heating in weak faults. Moreover, if the maximum increase in temperature is above a certain level (probably it is no more than 10 K), the permeability rather than the maximum increase in temperature becomes important for the lengthening effect. In addition, the degree of the dynamic undershoot and that of the energy radiation is larger in the case of sufficiently narrower slip zones. These phenomena originally derive from the limit of coseismic stress drop by the absolute level of pre-seismic stress.

These features do not depend on whether the assumed evolution law is the Ruina law or the Dieterich law. With either law, TP makes the recurrence interval be almost linearly proportional to the static stress drop.

However, we have found that the maximum friction in faults obeying the Dieterich law is increased by TP. From this result, we can consider that the ideal time-predictable model for earthquake cycles (*Shimazaki and Nakata* [1980]) would be inapplicable for faults obeying the Dieterich law, if the degree of TP is different for each earthquake event. By contrast, it can be applicable for faults obeying the Ruina law regardless of the degree of TP.

At last, it is a challenging and important problem to understand the role of TP in actual earthquakes. We have shown that we should measure the permeability rather than the thickness of the slip zone (or the increase in temperature) in order to estimate the effect of TP on long-term earthquake cycles. Although it is currently difficult to measure the permeability except near the ground surface, it is necessary to perform such measurements in light of their importance for predicting future seismic hazards. For instance, TP might be a dominant coseismic weakening mechanism for giant interplate earthquakes such as the Tokai, Tonankai and Nankai earthquakes in southwest Japan, even though the plate interfaces are considered to be weak (*Wang* [2000]; *Seno* [2009]).

Appendix A: Effects of the Linker-Dieterich term

Linker and Dieterich [1992] and subsequent experimental studies (e.g., *Richardson and Marone* [1999]) have revealed that the evolution of θ has a dependency on normal stress. Following their formulation, one term is added to equation (4) or to equation (5) as follows:

$$\frac{d\theta}{dt} = -\frac{v\theta}{L}\ln\left(\frac{v\theta}{L}\right) - \frac{D\theta}{b\bar{\sigma}}\frac{d\bar{\sigma}}{dt} \quad \text{(A1)}$$

$$\frac{d\theta}{dt} = 1 - \frac{v\theta}{L} - \frac{D\theta}{b\bar{\sigma}}\frac{d\bar{\sigma}}{dt} \quad \text{(A2)}$$

Table 5. Model parameters and numerical results in the case of the Ruina evolution law including the Linker-Dieterich term.

w [m]	R_i [year]	S_d [MPa]	S_s [MPa]	ΔT [K]	u_{cos} [m]	σ_a [MPa]	M
0.01	129.4	5.6	4.7	95	3.8	2.9	7.5
0.02	131.4	5.6	4.8	57	3.8	2.8	7.5
0.04	134.4	5.7	4.9	34	3.9	2.7	7.6
0.1	143.3	5.7	5.2	20	4.2	2.1	7.6
0.2	142.5	5.3	5.2	16	4.2	1.3	7.6
0.4	97.8	3.5	3.5	9.2	2.8	0.6	7.5
1.0	46.6	1.6	1.6	2.2	1.3	0.5	7.2
2.0	37.9	1.3	1.3	0.9	1.1	0.4	7.2
∞	32.0	1.1	1.1	0.0	0.9	0.4	7.1

where D is a constant and its typical value is 0.3 (*Richardson and Marone* [1999]).

In order to evaluate the effect of the Linker-Dieterich term, it is necessary to perform calculations using it with the Ruina law, $D = 0.3$ and $\kappa = 10^{-19}$ m^2. The results are listed in Table 5.

We notice that the results in Table 5 are rather similar to the results without the Linker-Dieterich term in Table 2. To cite a different point, the recurrence intervals are somewhat longer than those in Table 2. However, we can ignore this slight difference since the difference caused by the other factors, such as the thickness of the slip zone, the permeability or the evolution law of θ, is greater, as revealed in Section 3.

Appendix B: Ignored TP effect with extremely low slip velicity

In this study, shear heating with $v < v_0$ is ignored. It is necessary to check the validity of this assumption from the standpoint of the sensitivity of the pore pressure to the slip velocity.

Considering the case of the highest sensitivity in this study, we assume $w = \epsilon$ (most heatable for constant slip velocity and frictional stress) and $\kappa = 10^{-19}$ m^2 (highest sensitivity of pore pressure to constant heating). If we set the parameters in Table 1 and assume constant frictional stress $\tau_f = \tau_f^c = \mu_0[\sigma - p_0] = 6$ MPa for simplicity, the increase in pore pressure Δp [Pa] is approximately represented using equation (9) as follows:

$$\Delta p(t) \sim \frac{5\times10^5}{10\times10^6\times(\sqrt{10^{-6}}+\sqrt{10^{-4}})}\int_0^t \frac{\tau_f^c v(t_*)dt_*}{\sqrt{t-t_*}} \sim 5\times\int_0^t \frac{\tau_f^c v(t_*)dt_*}{\sqrt{t-t_*}} \quad \text{(B1)}$$

Moreover, for example, if the slip velocity is constant ($v = 0.1v_0 \sim 1\times10^{-10}$ m/s), equation (B1) can be rewritten as follows:

$$\Delta p(t) \sim 3\times10^{-3}\times\int_0^t \frac{dt_*}{\sqrt{t-t_*}} = 6\times10^{-3}\sqrt{t} \quad \text{(B2)}$$

As an example, even if the state of $v = 0.1v_0$ lasts for 100 year ($\sim 3\times10^9$ sec.), Δp is at most 400 Pa, which is sufficiently smaller than $\sigma - p_0 = 1\times10^7$ Pa.

Thus, it is not necessary to consider the effects of TP for extremely low slip velocity ($< v_0$), at least in this study.

Acknowledgments. We are grateful to A. Bizzarri and an anonymous reviewer for improving this paper. This research has been supported primarily by the Japan Society for the Promotion of Science (20-230) and a Grant-in-Aid for Scientific Research (B) (20340119) from MEXT.

References

Andrews, D. J. (2002), A fault constitutive relation accounting for thermal pressurization of pore fluid, *J. Geophys. Res.*, *107*(B12), doi:10.1029/2002JB001942.

Bizzarri, A., and M. Cocco (2006a), A thermal pressurization model for the spontaneous dynamic rupture propagation on a three-dimensional fault: 1. methodological approach, *J. Geophys. Res.*, *111*(B05303), doi:10.1029/2005JB003862.

Bizzarri, A., and M. Cocco (2006b), A thermal pressurization model for the spontaneous dynamic rupture propagation on a three-dimensional fault: 2. traction evolution and dynamic parameters, *J. Geophys. Res.*, *111*(B05304), doi:10.1029/2005JB003864.

Brace, W. F., and J. D. Byerlee (1966), Stick-slip as a mechanism for earthquakes, *Science*, *153*(3739), 990–992.

Brodsky, E. E., and H. Kanamori (2001), Elastodynamic lubrication of faults, *J. Geophys. Res.*, *106*(B8), 16,357–16,374.

Brune, J. N. (1970), Tectonic stress and spectra of seismic shear waves from earthquakes, *J. Geophys. Res.*, *75*, 4997–5009.

Cochard, A., and R. Madariaga (1994), Dynamic faulting under rate-dependent friction, *Pure Appl. Geophys.*, *142*, 419–445.

Dieterich, J. H. (1979), Modeling of rock friction 1. Experimental results and constitutive equations, *J. Geophys. Res.*, *84*(B5), 2161–2168.

Eshelby, J. (1957), The determination of the elastic field of an ellipsoidal inclusion and related problems, *Proc. Roy. Soc. Lond. A*, *242*, 376–396.

Fukuyama, E., and R. Madariaga (1998), Rupture dynamics of a planar fault in a 3D elastic medium: Rate- and slip- weakening friction, *Bull. Seis. Soc. Ame.*, *88*(1), 1–17.

Gu, Y., and T.-F. Wong (1991), Effects of loading velocity, stiffness, and inertia on the dynamics of a single degree of freedom spring-slider system, *J. Geophys. Res.*, *96*(B13), 21,677–21,691.

Guatteri, M., P. Spudich, and G. C. Beroza (2001), Inferring rate and state friction parameters from a rupture model of the 1995 Hyogo-ken Nanbu (Kobe) Japan earthquake, *J. Geophys. Res.*, *106*(B11), 26,511–26,521.

He, C., T.-F. Wong, and N. M. Beeler (2003), Scaling of stress drop with recurrence interval and loading velocity for laboratory-derived fault strength relations, *J. Geophys. Res.*, *108*(B1), doi:10.1029/2002JB001890.

Hirose, T., and T. Shimamoto (2005), Growth of molten zone as a mechanism of slip weakening of simulated faults in gabbro during frictional melting, *J. Geophys. Res.*, *110*(B05202), doi:10.1029/2004JB003207.

Ishikawa, T., et al. (2008), Coseismic fluid rock interactions at high temperatures in the chelungpu fault, *Nature Geoscience*, *1*, 679–683.

Kanamori, H., and L. Rivera (2006), Energy partitioning during an earthquake, in *Earthquakes*, edited by R. Abercrombie, A. McGarr, H. Kanamori, and G. Di Toro, AGU Geophysical Monograph 170, pp. 3–13.

Kano, Y., J. Mori, R. Fujio, H. Ito, T. Yanagidani, S. Nakao, and K.-F. Ma (2006), Heat signature on the Chelungpu fault associated with the 1999 Chi-Chi, Taiwan earthquake, *Geophys. Res. Lett.*, *33*(L14306), doi:10.1029/2006GL026733.

Kato, N. (2004), Interaction of slip on asperities: Numerical simulation of seismic cycles on a two-dimensional planar fault with nonuniform frictional property, *J. Geophys. Res.*, *109*(B12306), doi:10.1029/2004JB003001.

Kato, N., and T. E. Tullis (2001), A comoposite rate- and state-dependent law for rock friction, *Geophys. Res. Lett.*, *28*(6), 1103–1106.

Lachenbruch, A. H. (1980), Frictional heating, fluid pressure, and the resistence to fault motion, *J. Geophys. Res.*, *85*(B11), 6097–6112.

Linker, M. F., and J. H. Dieterich (1992), Effects of variable normal stress on rock friction: Observations and constitutive equations, *J. Geophys. Res.*, *97*(B4), 4923–4940.

Liu, Y., and J. R. Rice (2007), Spontaneous and triggered aseismic deformation transients in a subduction fault model, *J. Geophys. Res.*, *112*(B09404), doi:10.1029/2007JB004930.

Mase, C. W., and L. Smith (1987), Effects of frictional heating on the thermal, hydrologic, and mechanical response of a fault, *J. Geophys. Res.*, *92*(B7), 6249–6272.

Mayeda, K., R. Gök, W. R. Walter, and A. Hofstetter (2005), Evidence for non-constant energy/moment scaling from coda-derived source spectra, *Geophys. Res. Lett.*, *32*(L10306), doi: doi:10.1029/2005GL022405.

Miyazaki, S., P. Segall, J. Fukuda, and T. Kato (2004), Space time distribution of afterslip following the 2003 Tokachi-oki earthquake: Implications for variations in fault zone frictional properties, *Geophys. Res. Lett.*, *31*(L06623), doi: 10.1029/2003GL019410.

Nakatani, M. (2001), Conceptual and physical clarification of rate and state friction: Frictional sliding as a thermally activated rheology, *J. Geophys. Res.*, *106*(B7), 13,347–13,380.

Otsuki, K., N. Monzawa, and T. Nagase (2003), Fluidization and melting of fault gouge during seismic slip: Identification in the Nojima fault zone and implications for focal earthquake mechanisms, *J. Geophys. Res.*, *108(B4)*(2192), doi: 10.1029/2001JB001711.

Pittarello, L., G. Di Toro, A. Bizzarri, G. Pennacchioni, J. Hadizadeh, and M. Cocco (2008), Energy partitioning during seismic slip in pseudotachylyte-bearing faults (Gole Larghe Fault, Adamello, Italy), *Earth. Planet. Sci. Lett.*, *269*, 131–139.

Press, W. H., B. P. Teukolsky, and W. T. Vetterling (1992), *Numerical Recipes*, 2nd ed., Cambridge University Press, New York.

Rice, J. R. (1993), Spatio-temporal complexity of slip on a fault, *J. Geophys. Res.*, *98*(B6), 9885–9907.

Rice, J. R. (2006), Heating and weakening of faults during earthquake slip, *J. Geophys. Res.*, *111*(B05311), doi: 10.1029/2005JB004006.

Rice, J. R., and S. T. Tse (1986), Dynamic motion of a single degree of freedom system following a rate and state dependent friction law, *J. Geophys. Res.*, *91*(B1), 521–530.

Richardson, E., and C. Marone (1999), Effects of normal stress vibrations on frictional healing, *J. Geophys. Res.*, *104*(B12), 28,859–28,878.

Ruina, A. (1983), Slip instability and state variable friction laws, *J. Geophys. Res.*, *88*(B12), 10,359–10,370.

Ruina, A. L. (1980), Friction laws and instabilities: A quasistatic analysis of some dry frictional behavior, Ph.D. thesis, Cornell University.

Seno, T. (2009), Determination of the pore fluid pressure ratio at seismogenic megathrusts in subduction zones: Implications for strength of asperties and Andean-type mountain building, *J. Geophys. Res.*, *114*(B05405), doi:10.1029/2008JB005889.

Shimazaki, K., and T. Nakata (1980), Time-predictable recurrence model for large earthquakes, *Geophys. Res. Lett.*, *7*(4), 279–282.

Shiption, Z. K., A. M. Soden, J. D. Kirkpatrick, A. M. Bright, and R. J. Lunn (2006), How thick is a fault? Fault displacement-thickness scaling revisited, in *Earthquakes*, edited by R. Abercrombie, A. McGarr, H. Kanamori, and G. Di Toro, AGU Geophysical Monograph 170, pp. 193–198.

Sibson, R. H. (1973), Interactions between temperature and fluid pressure during earthquake faulting a mechanism for partial or total stress relief, *Nature*, *243*, 66–68.

Sibson, R. H. (2003), Thickness of the seismic slip zone, *Bull. Seism. Soc. Am.*, *93*(3), 1169–1178.

Suzuki, T., and T. Yamashita (2006), Nonlinear thermoporoelastic effects on dynamic earthquake rupture, *J. Geophys. Res.*, *111*(B03307), doi:10.1029/2005JB003810.

Tanaka, H., W. M. Chen, C. Y. Wang, K. F. Ma, N. Urata, J. Mori, and M. Ando (2006), Frictional heat from faulting of the 1999 Chi-Chi, Taiwan earthquake, *Geophys. Res. Lett.*, *33*(L16316), doi:10.1029/2006GL026673.

Tse, S. T., and J. R. Rice (1986), Crustal earthquake instablity in relation to the depth variation of frictional slip properties, *J. Geophys. Res.*, *91*(B9), 9452–9472.

Tsutsumi, A., S. Nishino, K. Mizoguchi, T. Hirose, S. Uehara, K. Sato, W. Tanikawa, and T. Shimamoto (2004), Pricipal fault zone width and permeability of the active Neodani fault, Nobi fault system, Southwest Japan, *Tectonophysics*, *379*, 93–108.

Wang, K. (2000), Stress-strain 'paradox', plate coupling, and forearc seismicity at the Cascadia and Nankai subduction zones, *Tectonophysics*, *319*, 321–338.

Wibberley, C. A. J., and T. Shimamoto (2003), Internal structure and permeability of major strike-slip fault zones: the Median Tectonic Line in Mie Prefecture, Southwest Japan, *J. Struct. Geol.*, *25*, 59–78.

Yuta Mitsui

Department of Geophysics, Graduate School of Science, Kyoto University, Kitashirakawa-Oiwakecho, Sakyo, Kyoto 606-8224, Japan (mitsui@kugi.kyoto-u.ac.jp)